Patel, A.K., Yadav, R.P., Majava, V., Kursula, I., Kursula, P.

Structure of the dimeric autoinhibited conformation of DAPK2, a pro-apoptotic protein kinase

(2011) Journal of Molecular Biology, 409 (3), pp. 369-383

doi:10.1016/j.jmb.2011.03.065 J. Mol. Biol. (2011) 409, 369–383

Contents lists available at www.sciencedirect.com

Journal of Molecular Biology

journal homepage: http://ees.elsevier.com.jmb

Structure of the Dimeric Autoinhibited Conformation of DAPK2, a Pro-Apoptotic Protein Kinase

Ashok K. Patel[1]†, Ravi P. Yadav[2]†, Viivi Majava[1], Inari Kursula[2] and Petri Kursula[1,2]*

[1]*Department of Biochemistry, University of Oulu, 90014 Oulu, Finland*
[2]*Centre for Structural Systems Biology, Helmholtz Centre for Infection Research (CSSB-HZI), DESY, 22607 Hamburg, Germany*

Received 18 February 2011; received in revised form 24 March 2011; accepted 28 March 2011
Available online 8 April 2011

Edited by M. Guss

Keywords:
crystallography;
autoinhibition;
small-angle X-ray scattering;
dimerization;
active site

The death-associated protein kinase (DAPK) family has been characterized as a group of pro-apoptotic serine/threonine kinases that share specific structural features in their catalytic kinase domain. Two of the DAPK family members, DAPK1 and DAPK2, are calmodulin-dependent protein kinases that are regulated by oligomerization, calmodulin binding, and autophosphorylation. In this study, we have determined the crystal and solution structures of murine DAPK2 in the presence of the autoinhibitory domain, with and without bound nucleotides in the active site. The crystal structure shows dimers of DAPK2 in a conformation that is not permissible for protein substrate binding. Two different conformations were seen in the active site upon the introduction of nucleotide ligands. The monomeric and dimeric forms of DAPK2 were further analyzed for solution structure, and the results indicate that the dimers of DAPK2 are indeed formed through the association of two apposed catalytic domains, as seen in the crystal structure. The structures can be further used to build a model for DAPK2 autophosphorylation and to compare with closely related kinases, of which especially DAPK1 is an actively studied drug target. Our structures also provide a model for both homodimerization and heterodimerization of the catalytic domain between members of the DAPK family. The fingerprint of the DAPK family, the basic loop, plays a central role in the dimerization of the kinase domain.

**Corresponding author.* CSSB-HZI, DESY, Notkestrasse 85, D-22607 Hamburg, Germany. E-mail address: petri.kursula@desy.de.

† A.K.P. and R.P.Y. contributed equally to this work.

Present addresses: A. K. Patel, Department of Biophysics, Johns Hopkins University, Baltimore, MD 21218, USA; R. P. Yadav, Molecular Biology Unit, Institute of Medical Sciences, Banaras Hindu University, Varanasi 221005, India.

Abbreviations used: DAPK, death-associated protein kinase; CaM, calmodulin; CaMK, CaM-dependent protein kinase; SAXS, small-angle X-ray scattering; MLCK, myosin light chain kinase; PhK, phosphorylase kinase; EDTA, ethylenediaminetetraacetic acid; ZIPK, zipper-interacting protein kinase; ESRF, European Synchrotron Radiation Facility; EMBL/DESY, European Molecular Biology Laboratory/Deutsches Elektronen Synchrotron; BSA, bovine serum albumin; AMP-PNP, denosine 5'-(beta,gamma-imido)triphosphate.

Introduction

Death-associated protein kinases (DAPKs) are a family of five enzymes that share a high degree of sequence homology in their catalytic domains and function in the triggering of cellular apoptosis.[1] Two of the family members, DAPK1 and DAPK2, are calmodulin (CaM)-dependent protein kinases (CaMKs) that are activated by CaM in response to Ca^{2+} stimuli.[2–4] These kinases are kept in an inactive state by a double-locking mechanism, which requires dephosphorylation of an autophosphorylated residue within the CaM-binding domain, Ser308, and CaM binding for kinase activation.[5,6]

DAPK2 has, in addition to the kinase domain, an autoinhibitory region, a CaM-binding segment, and a 40-residue C-terminal region suggested to be involved in enzyme dimerization.[5] The C-terminal tail is predicted to form two helices and has no detectable sequence homology to known protein sequences. The physiological substrate of DAPK2 is unknown, although it phosphorylates the myosin light chain *in vitro*.[7] However, in light of the high homology to DAPK1 in the catalytic domain, it is likely that the substrate preferences for both kinases are similar and that differences in their actions are governed to a large extent by differences in expression profiles, interactions with specific regulators, and subcellular localization.

Originally, DAPK2 was shown to be involved in type II autophagic cell death, during which it localizes specifically in the lumen of autophagic vesicles.[7] It is involved in the caspase-independent process of membrane blebbing observed in this mode of cell death.[7] In recent years, more data with regard to the biological function of DAPK2 have become available. For example, it has been shown to be involved in the regulation of erythropoiesis[8] and granulocyte maturation.[9] Furthermore, the inhibition of fatty acid synthase in cancer cells leads to apoptosis through a pathway, in which DAPK2 is likely to be involved.[10] Recently, the pro-apoptotic properties of DAPK2 have been utilized in pilot studies aiming at the development of immunokinases, fusion proteins that are targeted to defined cancer cells with the purpose of triggering apoptosis.[11] In Hodgkin lymphoma cells, DAPK2 is downregulated, and the restoration of its activity through an immunokinase approach, by way of fusing CD30 ligand and a constitutively active DAPK2, leads to selective apoptosis in tumors.[12]

Drug design within the DAPK family is mainly being actively carried out on the basis of the structure of the active DAPK1 conformation.[13–21] DAPK1 is a promising target for drug development, especially with the aim of interfering with neuronal apoptosis after stroke. Structures of closely related kinases from the DAPK family should be of importance in such endeavors.

Here, the first crystal structures of DAPK2 are reported. Although peptide binding is blocked by the autoinhibitory helix, the ATP-binding site is accessible, and the αC helix is in the active conformation. Comparison of the structure to that of other CaM-dependent kinases allows us to develop a more detailed picture of DAPK regulation. Based on the structure, we can further propose a model for DAPK2 autophosphorylation and the role of the observed dimerization in the crystal and solution states in DAPK2 regulation.

Results and Discussion

Purification of monomeric and dimeric forms of DAPK2

Mouse recombinant full-length DAPK2 was expressed and purified, and when subjected to size-exclusion chromatography, it presented two main peaks, corresponding to the sizes of a

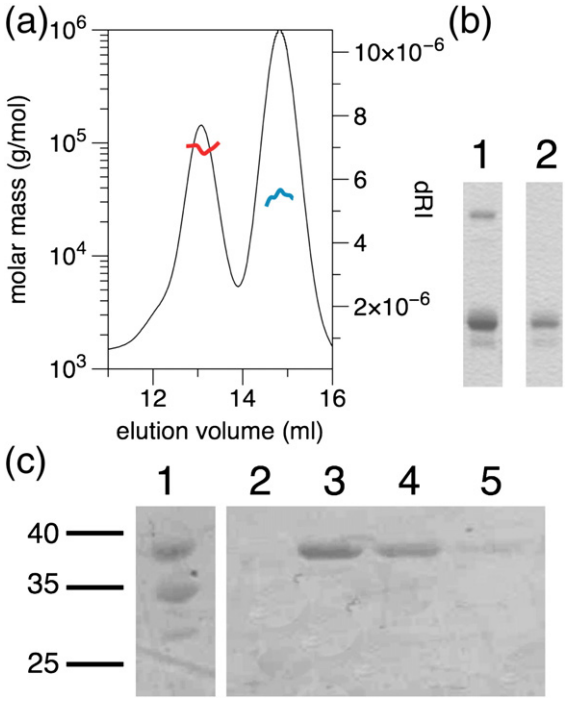

Fig. 1. Purification and characterization of recombinant DAPK2. (a) Size-exclusion chromatography showing two peaks, which were shown to correspond to monomeric and dimeric forms by static light scattering. (b) SDS-PAGE analysis of fractions from the dimeric (lane 1) and monomeric (lane 2) fractions showing stable dimers in the dimeric peak. Compared to markers, the sizes correspond to approximately 42 kDa and 90 kDa. (c) Purification of DAPK2 by CaM-affinity chromatography. The starting sample (lane 1) contained, in addition to the full-length protein, two degradation products. When the sample was bound to CaM agarose in the presence of calcium and eluted with EDTA (lanes 2–5), only the full-length protein was observed. The molecular masses of standard proteins (in kilodaltons) are indicated on the left.

monomer and a dimer (Fig. 1a). When analyzed by electrophoresis under denaturing conditions (Fig. 1b), both peaks contained a protein corresponding to the size of DAPK2; in addition, the dimer peak showed a dimer on electrophoresis, resistant to the denaturing conditions employed. To get further insight into the molecular weights of the molecular species in the two peaks, we used static light scattering to determine the absolute molar mass (Fig. 1a). The result, again, showed that the dimer peak had a molar mass approximately twice that of the monomeric peak. The monomeric and dimeric fractions were kept separate after purification and used further for solution structure determination by small-angle X-ray scattering (SAXS) (see below).

Full-length DAPK2, from the monomeric fraction, could be further purified using calcium-dependent affinity chromatography on CaM agarose. While the starting sample for this specific experiment contained two degradation products, these were no longer detected in the fractions eluted from the CaM matrix with ethylenediaminetetraacetic acid (EDTA) (Fig. 1c). This indicates that (a) the full-length recombinant DAPK2 binds to CaM in a calcium-dependent manner and that (b) the degradation products have lost, at least partially, their CaM-binding domain located at residues 302–320. It has been shown before that DAPK2 containing residues 1–320 is able to bind to CaM and get activated.[5] The full-length DAPK2 purified by CaM affinity was further used for crystallization.

Overall crystal structure of apo DAPK2

The crystal structure of unliganded mouse DAPK2 was refined at 2.3 Å resolution. It has the typical protein kinase fold, comprising an N-terminal small lobe and a C-terminal large lobe, between which reside the nucleotide-binding cleft and the catalytic site (Fig. 2a). The kinase is well defined in electron density up to residue 301, that is, including the autoinhibitory domain but not the CaM-binding site; judging from crystal packing, there is no room for the 60 C-terminal residues. Thus, the crystallized protein most likely represents the main degradation product observed for DAPK2 during purification, before the CaM-affinity step (Fig. 1c). This is despite the fact that the CaM-affinity purified full-length DAPK2 was used for crystallization, presenting only a single protein band on SDS-PAGE prior to crystallization. It is likely that the full-length protein is unstable and has further degraded during crystallization to yield a smaller fragment, which has lost the CaM-binding domain. Nevertheless, the structure of DAPK2 with the autoinhibitory domain was obtained.

As expected, in light of the high sequence homology to the catalytic domain of DAPK1, the

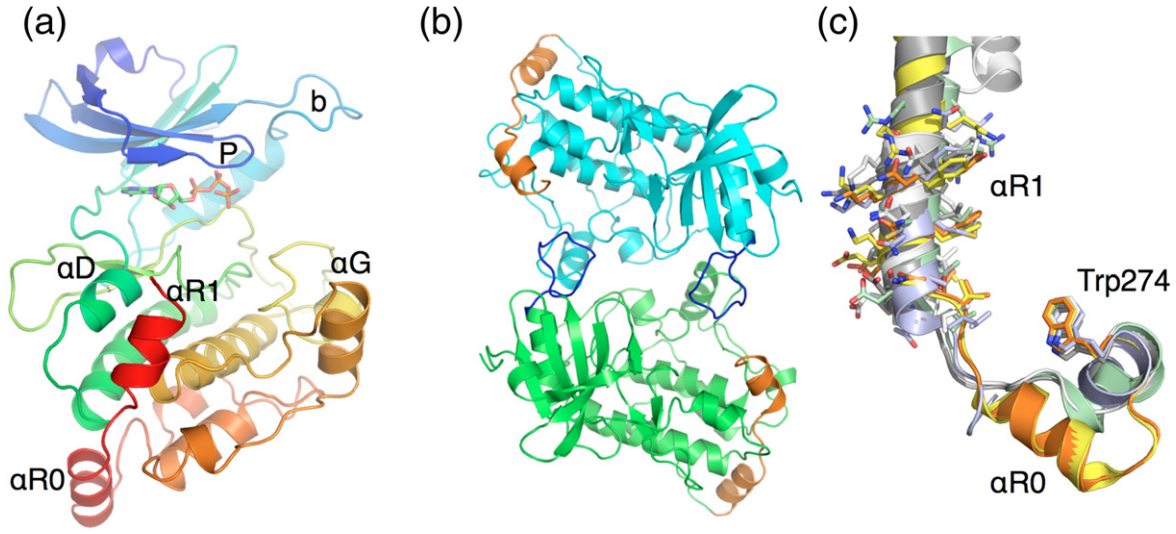

Fig. 2. The crystal structure of DAPK2. (a) The monomeric DAPK2, indicating the location of the ATP-binding site and the autoinhibitory domain (in red). The protein is colored from blue (N terminus) to red (C terminus). P, P-loop; b, basic loop. (b) The dimeric arrangement of DAPK2 in the asymmetric unit. The two monomers are colored green and cyan, and the autoinhibitory domains are shown in orange. The basic loop is indicated in blue. (c) The autoinhibitory domain from several known structures of autoinhibited CaMK family members. The conserved Trp residue (Trp274 in DAPK2), marking the end of the catalytic core domain, is on the bottom right. The kinases are as follows: DAPK2, orange; DAPK1,[22] yellow; CaMK1,[23] white; CaMK2,[24] gray; CaM-activated serine/threonine kinase,[25] green; and calcium-dependent protein kinase 3,[26] blue. Note the linker region containing the three-turn αR0 helix (bottom) present in the DAPK family kinases between the kinase domain and the autoinhibitory helix αR1. More detailed views are shown in Fig. 3.

overall structure of DAPK2 closely resembles that of DAPK1. The αC helix of the N-terminal lobe is in the active conformation, in contrast to previously determined structures for the autoinhibited conformations of the titin and twitchin kinases.[27,28] The salt bridge characteristic of the active conformation of a protein kinase is formed between the DAPK2 active-site ATP-coordinating residue Lys42 and Glu64 from the αC helix. In autoinhibited CaMK1, the αC helix is partly disordered, and this ion pair is not formed—probably because the CaM-binding domain distorts the N-terminal lobe.[23] In autoinhibited CaMK2, this ion pair is present,[24] while in the inhibited conformation of the DAPK1–CaM complex, it is broken.[22] This indicates that, despite the presence of the autoinhibitory domain, the active site of DAPK2 is in a catalytically competent conformation. The presence of an active conformation is likely to be of importance in DAPK2 autophosphorylation.

The autoinhibitory domain and the substrate peptide-binding site

The autoinhibitory region in CaMKs between the catalytic domain and the CaM-binding region plays a central role in kinase regulation. In CaMK1,[23] CaM-activated serine/threonine kinase,[25] titin kinase,[27] and twitchin kinase,[28] this region contains an autoinhibitory α-helix at the same position. In the DAPK2 structure, the autoinhibitory region is formed by two helices, αR0 and αR1; the latter corresponds to the autoinhibitory helix seen in the aforementioned kinases (Fig. 2c). In crystal structures of both autoinhibited CaMK2[24] and DAPK1,[22] the autoinhibitory segment forms a long continuous helix together with the CaM-binding domain; the same is true for the inhibited conformation of the homologous calcium-dependent protein kinase 3 from *Toxoplasma gondii* bound to its C-terminal CaM-like regulatory domain.[26] In all these kinases, the autoinhibitory helix runs in a similar cleft toward the substrate-binding surface and active site, pushing away helix αD (Figs. 2a and 3c). When the catalytic domains of DAPK2 and related kinases are superimposed, the autoinhibitory helices overlap in the same orientation, although not in completely the same register (Fig. 3a and b). Studies using mutagenesis to disrupt the autoinhibitory helix in myosin light chain kinase (MLCK)[29] and CaMK2[30] have indicated that its secondary structure is important for autoinhibition and CaM-dependent activation. For smooth muscle MLCK, truncation studies have indicated that the region corresponding up to residue 300 in DAPK2, just before the stretch of three basic residues at the start of the CaM-binding domain, is crucial for autoinhibition.[31] This segment corresponds exactly to the region seen in our crystal structure of DAPK2. Thus, the autoinhibitory helix in all these kinases sterically blocks the peptide-binding site by making both hydrophobic and electrostatic contacts with the kinase core. Binding of CaM to a CaM-dependent kinase results in pulling away of the autoinhibitory helix and kinase activation.

The autoinhibitory region of DAPK2 can be divided into two parts: a linker region (residues 277–291) with unknown relevance and the autoinhibitory helix αR1 necessary for autoinhibition (residues 292–301). In DAPK2, the linker region is composed of a helix (residues 280–289) αR0, previously not seen in CaM kinase structures other than that of DAPK1,[22] and a short β-strand (residues 289–291) forming a small antiparallel β-sheet with residues 111–113 (from the αD–αE loop) and 243 (from the αG–αH loop) of the kinase core. The latter region in the kinase core probably recognizes positively charged residues in the substrate around positions P-6 to P-8.[17]

While the linker region varies between different CaM kinases in sequence, structure, and length, the autoinhibitory helix αR1 is present in all of them, and basic and hydrophobic residues in it are conserved (Fig. 2c and 3a and b).[22] The conserved residues are oriented such that the hydrophobic residues anchor the autoinhibitory helix to the kinase C-terminal lobe, while the basic residues give the outer surface of the autoinhibitory helix a positive charge. While the spatial locations of the conserved residues are highly similar, their exact positions in the amino acid sequence are not fully conserved.

The conserved basic residues, Lys297 and Lys298 in DAPK2, on the outside surface of the autoinhibitory helix may be important for CaM recognition. Such a role for basic residues outside the minimal CaM-binding sequence has been proposed based on mutagenesis studies on MLCK.[32] When we look at known structures of autoinhibited CaMKs, it is evident that two or three such residues are always present on the outside of the autoinhibitory helix (Fig. 3a). A superposition of CaMKs having the autoinhibitory helix also indicates the presence of a conserved acidic residue on the outside of the helix; in DAPK2, this residue is Glu294 (Fig. 3a). It is possible that such a feature plays a role in defining the boundary of the binding site for CaM, which has a high negative surface charge.

Between the autoinhibitory helix and the kinase core, Phe296 is a major hydrophobic anchor residue for DAPK2, being buried deep in a hydrophobic pocket of the DAPK2 C-terminal lobe (Fig. 3b). Phe296 is conserved between DAPK1 and DAPK2 but is an aliphatic residue in other known structures. Another conserved hydrophobic anchor is Tyr300 in DAPK2; interestingly, in all other kinases used for the comparison, including the highly homologous DAPK1, this anchor is Phe, located one position earlier in the amino acid sequence. Tyr300 interacts with Phe102 through an edge-to-face CH–π bond

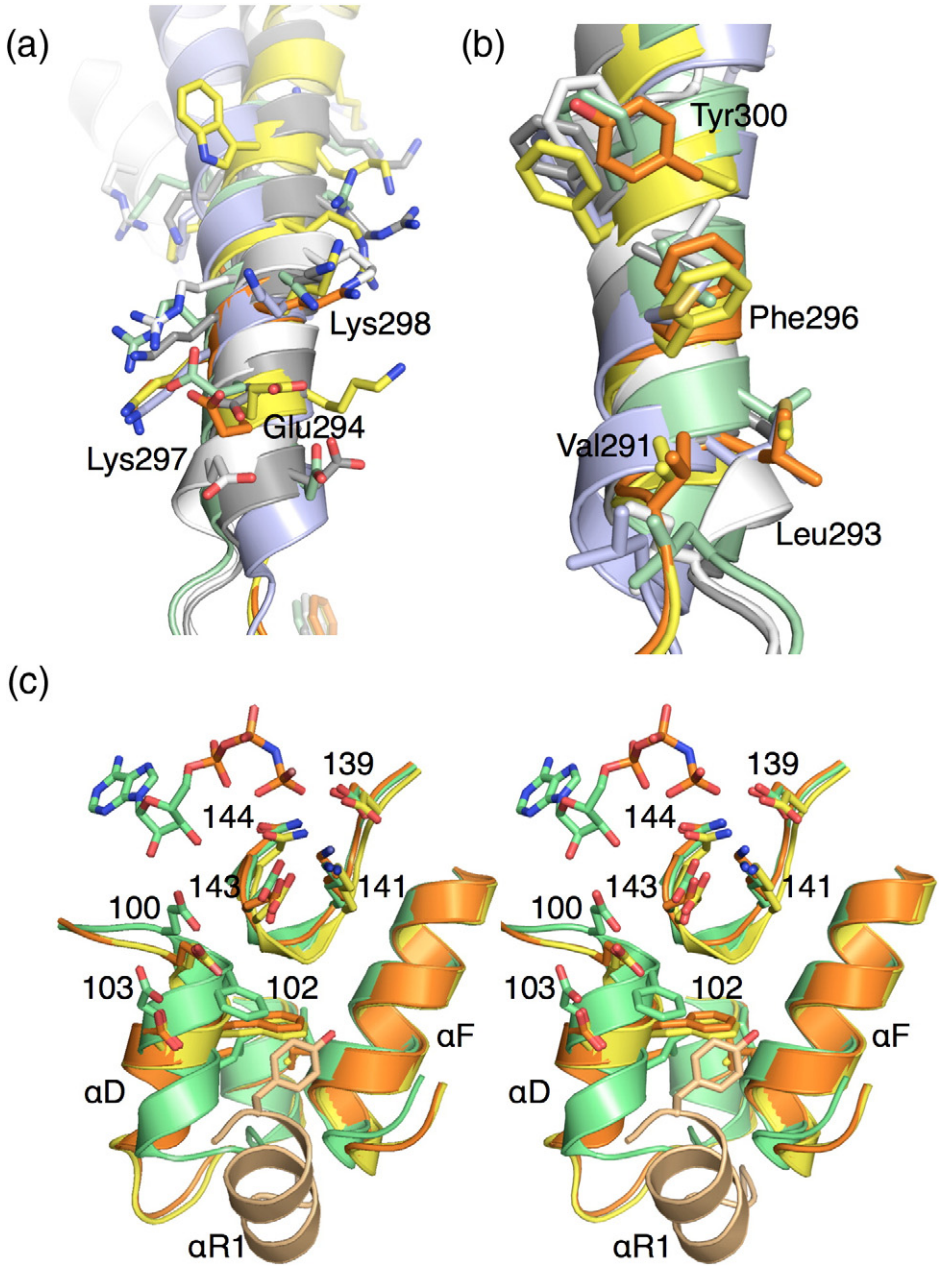

Fig. 3. Details of the autoinhibitory helix of DAPK2. (a) A view from the outside of the autoinhibitory helix of DAPK2 and related kinases. Coloring is as in Fig. 2c. A cluster of basic residues is seen at the upper part of the autoinhibitory helix (Trp305 of DAPK1 can be seen as the upper boundary of this region), while at the bottom region, conservation of an acidic character is observed. The positions of Glu294, Lys297, and Lys298 in DAPK2 are indicated. (b) The hydrophobic anchors of the autoinhibitory helix, view from the side of the catalytic core domain. The two main anchor sites correspond to Phe296 and Tyr300 of DAPK2. While Phe296 is conserved between DAPK1 and DAPK2, Tyr300 is unique for DAPK2. The DAPK2 hydrophobic anchors are numbered. (c) An overview (in stereo) of the conformational changes between the inhibited and the active conformations. DAPK2, orange (autoinhibitory helix in light orange); DAPK1–CaM inactive complex, yellow; and DAPK1 catalytic domain, green. The AMP-PNP molecule in the catalytic domain of DAPK1 is also shown.[20] The largest differences concern helix αD, including the flipping out of Phe102 in the absence of the autoinhibitory tail.

where the edge of the Phe102 ring points at the face of the Tyr300 aromatic ring. Val291 and Leu293 of the tail also interact with the hydrophobic pocket. The pocket for these hydrophobic interactions is lined by helices αD and αF and the loops that follow after them.

The autoinhibitory helix is also thought to be a mimic of the substrate peptide in trans-

phosphorylation (a "pseudosubstrate"), and a number of acidic residues in the kinase C-terminal lobe interacting with the autoinhibitory helix are also implicated in substrate recognition. As an example, Glu182 is expected to interact with the P-2 residue of the substrate,[17] most likely forming a salt bridge to an arginine or a lysine residue in this position. In DAPK2, the cluster of basic residues at positions 302–304 and 306 most likely interacts with Glu182. An electrostatic contact between the autoinhibitory region and the corresponding acidic residue at the peptide-binding surface is seen in the structure of twitchin kinase.[28]

The autoinhibitory domain causes local changes in conformation within the C-terminal lobe when compared to the active conformation, as seen in the structures of the catalytic domain of DAPK1.[21] Especially, helix αD of the C-terminal lobe is displaced, resulting also in changes in the peptide-binding region near the active site (Fig. 3c). The N terminus of this helix harbors an important residue, Glu100, a key determinant of substrate specificity at substrate peptide position P-3. Glu100 is hydrogen bonded to ATP in the DAPK1 structure,[21] and it is also conserved in Ser/Thr kinases having a substrate requirement of Arg in the P-3 position.[17] Indeed, the corresponding residue forms a salt bridge to the P-3 arginine of the peptide substrate in the phosphorylase kinase (PhK) ternary complex structure,[33] and this is probably common to other related kinases as well. In the case of the autoinhibited structure of CaMK1, a salt bridge is present between the corresponding residue, Glu102, and Lys300 of the regulatory tail.[23] In DAPK1 complexed with CaM but still in an inactive conformation,[22] Lys304 from the basic cluster between the autoinhibitory helix and the CaM-binding domain similarly forms a salt bridge to the nearby Asp103. In comparison of the autoinhibited DAPK2 conformation and the catalytic domain of DAPK1, a conformational change in Glu100 is seen, driving its side chain slightly further away from the nucleotide-binding site in the autoinhibited conformation. A major conformational change between the autoinhibited and the active states concerns Phe102, which flips out in the absence of the autoinhibitory domain (Fig. 3c).

A clear difference between DAPK1 and DAPK2 is observed in the peptide-binding surface, around Phe178. This is the activation loop region in many kinases; in DAPK1 and DAPK2, there is no evidence for a regulatory mechanism involving changes in the activation loop. The activation segment is one of the two "fingerprint" regions of the DAPK family, sharing little homology to other kinases.[21] Interestingly, this is the exact region that is expected to form a short β-sheet with the substrate to be phosphorylated and lining a pocket for a hydrophobic residue in the P+1 position. Between the active DAPK1 and the inactive DAPK2 conformations, the backbone of this loop changes, and some side chains move; most notably, the side chains of Phe178 and Ile177 flip to the other side of the main chain, such that, in the structure of the catalytic domain of DAPK1, the P+1 pocket appears to be lost. Interestingly, in the ternary peptide complex of PhK, this region is in the same conformation as in DAPK2, indicating an active conformation.[33] Moreover, in the DAPK2 apo structure, an oxidized DTT molecule was seen in the electron density and modeled into the P+1 pocket of each monomer (not shown). It acts as a mimic of a large hydrophobic/aromatic side chain, such as Phe (in the case of autophosphorylation, corresponding to Phe309 of DAPK2); upon soaking in nucleotides in the absence of added DTT, the DTT molecule is lost from the pocket, and small changes are seen in the conformation in the P+1 binding pocket (not shown). These differences at the peptide-binding site between DAPK2 (and PhK) and DAPK1 indicate that care should be taken when using the crystal structures of the catalytic domain of DAPK1 for purposes such as molecular docking and drug design.

The nucleotide-bound active site

In addition to the apo form, the DAPK2 structure was also solved in the presence of bound nucleotides, ATP (2.3 Å) and AMP (1.9 Å) (Table 1). The high occupancy of the ligand in both cases indicates that the presence of the autoinhibitory domain does not prevent nucleotide substrate binding (Fig. 4a and Supplementary Fig. 1). This is, in fact, logical, considering the fact that DAPK2 is able to autophosphorylate its regulatory tail, including residues within the CaM-binding domain.[5] For such an autophosphorylation, the autoinhibitory helix must be in the inhibitory conformation for Ser308 to reach the catalytic site.

Surprisingly, the two active sites of the dimer have different conformations in the presence of bound nucleotide (Fig. 4a). In one of the two monomers, the salt bridge between Lys42 and Glu64 is broken. Simultaneously, the conformation of the bound nucleotide is different, and changes are also observed in the surrounding solvent organization. In consideration of the ATP conformation when compared to earlier structures such as the DAPK–denosine 5'-(beta,gamma-imido)triphosphate (AMP-PNP) complex,[20] it can be seen that one of the conformations corresponds to the catalytically competent, productive binding mode, while the other conformation is more extended, and phosphorylation would not occur. In this nonproductive mode of binding, the salt bridge between Lys42 and Glu64 is lost. Intriguingly, the same phenomenon of two active-site conformations is seen with both AMP and ATP. Differences between the two active sites are not detectable in

Table 1. Crystallographic data collection and refinement

	DAPK2 apo	DAPK2 AMP	DAPK2 ATP
Beamline	ID14-2 ESRF	X12 EMBL/DESY	X12 EMBL/DESY
Wavelength (Å)	0.933	1.0	1.0
Space group	$P2_12_12_1$	$P2_12_12_1$	$P2_12_12_1$
Unit cell dimensions *a*, *b*, *c* (Å)	64.0, 86.4, 124.3	63.1, 85.4, 124.0	63.1, 86.0, 124.4
Data processing			
Resolution range (Å)[a]	50–2.30 (2.36–2.30)	50–1.90 (1.95–1.90)	40–2.30 (2.36–2.30)
R_{sym} (%)	9.1 (44.3)	9.8 (71.4)	8.4 (47.6)
$\langle I/\sigma I \rangle$	16.9 (4.6)	15.2 (2.3)	17.4 (4.2)
Completeness (%)	97.2 (97.8)	99.3 (97.5)	97.6 (97.8)
Redundancy	7.9 (8.1)	7.1 (5.1)	7.1 (6.8)
Structure refinement			
R_{work}/R_{free} (%)	20.6/26.1	17.2/21.5	21.6/27.1
rmsd bond distances (Å)	0.006	0.006	0.004
rmsd bond angles (°)	0.92	1.02	0.77
MolProbity analysis			
Clashscore (percentile)	8.08 (97th)	3.25 (98th)	12.58 (86th)
Ramachandran favored, disallowed (%)	98.3, 0.0	98.2, 0.0	98.0, 0.0
MolProbity score (percentile)	1.87 (94th)	1.41 (97th)	2.21 (80th)

The geometry was analyzed with MolProbity.[34]
[a] The data in parentheses correspond to the high-resolution shell.

the apo form, which was not soaked in nucleotide ligands, and thus, the specific conformational changes occurred during ligand soaking in the crystal state. It is worth noting that, in the autoinhibited DAPK1–CaM complex, the Lys42–Glu64 salt bridge is also broken.[22] The result indicates flexibility in the active-site structure upon nucleotide binding; it is possible that one reason for these changes is the omission of divalent cations from the nucleotide soaking experiments. The detected active-site flexibility is not restricted to the nucleotide and Lys42; also, the solvent structure around Lys42 is affected (Fig. 4a). Thus, even though the active site of DAPK2 seems to be pre-organized for catalysis without bound nucleotide, it actually can change toward an inactive state upon nucleotide binding.

Dimerization and the basic loop

The regulation of DAPK2 activity involves dimerization,[5] and the catalytic domains of the closely related DAPK1 and zipper-interacting protein kinase (ZIPK) kinases have been shown to heterodimerize in a signaling complex.[35] Furthermore, recently, the catalytic domain of DAPK1 was reported to dimerize.[36] A visual analysis of the packing of DAPK2 in the unit cell reveals that the lattice is formed of symmetrical dimers generated by a local non-crystallographic 2-fold rotation axis (Fig. 2b). The total buried solvent-accessible surface area at the dimer interface is over 3000 Å^2—very large for a nonspecific crystal contact but normal for a homodimer.[37] It is clear that, in this dimeric conformation, substrate peptide binding is impossible, and dimerization, as seen in the crystalline state, provides a logical model for DAPK2 autoinhibition. Whether the dimer seen in the crystal state represents the dimeric form observed in solution during purification was further confirmed by SAXS experiments (see below).

The DAPK family kinases have a unique basic loop next to the P-loop, preceding helix αC (Fig. 4b); this is the second fingerprint region of the DAPK family. The role of this conserved loop in catalysis, substrate recognition, or kinase regulation is not known. Mutating basic residues in this loop to alanine in the DAPK catalytic domain had no effect on substrate phosphorylation.[17] The loop has, however, been implicated both in the heterodimerization of DAPK1 and ZIPK[35] and in the homodimerization of the DAPK1 catalytic domain.[36] When looking at the kinase monomers in the DAPK2 and DAPK1 structures, we found that this loop makes very few contacts with the rest of the enzyme. On the other hand, if the dimeric arrangement—seen here in the crystal state for DAPK2—is considered, the basic loop inserts deep into a groove close to the active site in the opposing monomer, making a number of hydrogen-bonding contacts—mainly through Arg residues 47, 50, and 53—and van der Waals interactions. The basic loop is sandwiched in a pocket between helix αG and the autoinhibitory helix αR1, close to the active site of both monomers (Fig. 4b). One of the interactions seen for the basic loop is a salt bridge from Arg50 to Asp220 located in the N-terminal end of helix αG. Of note, also the other fingerprint region of the DAPK

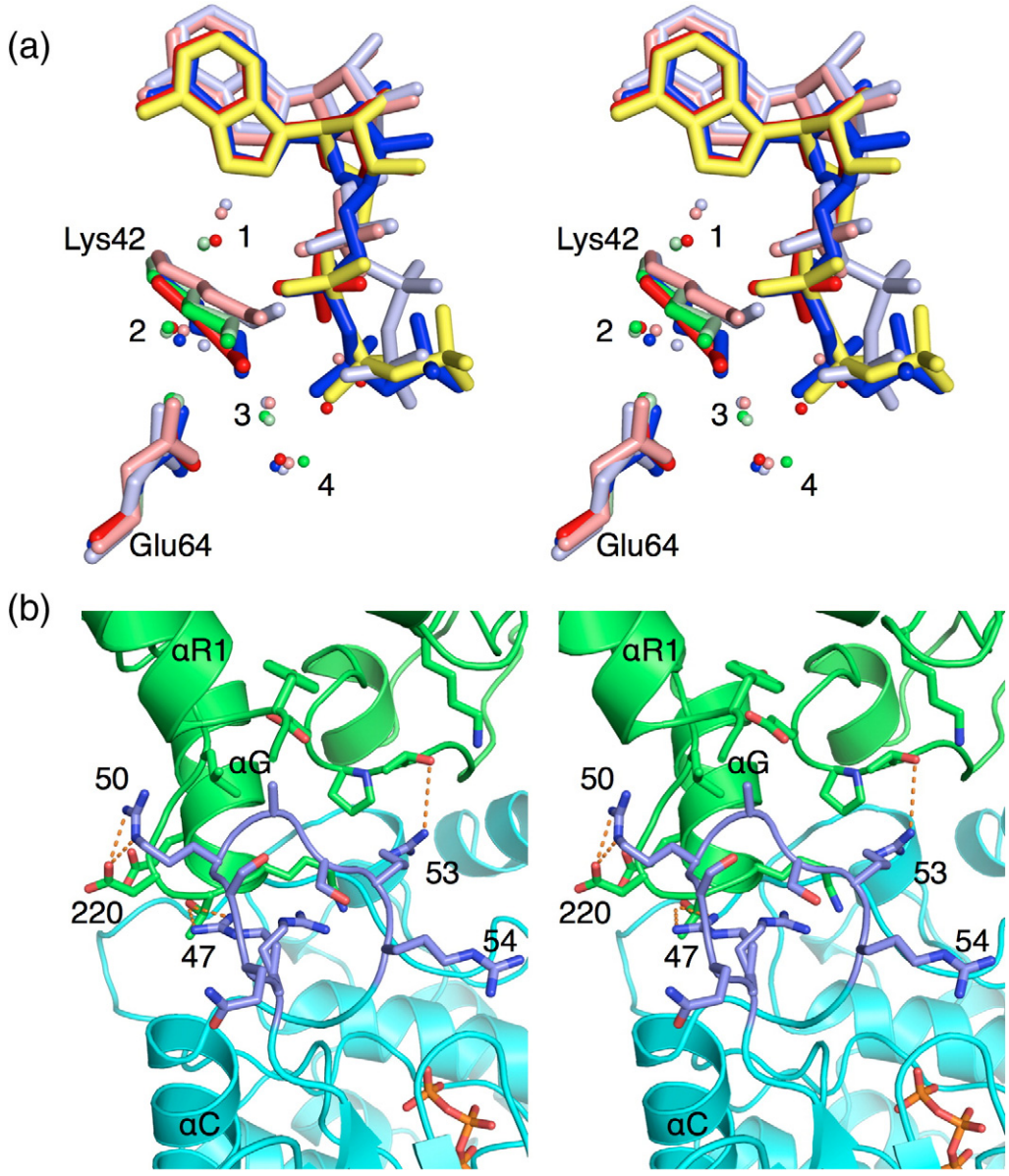

Fig. 4. The active site and the basic loop. (a) Two conformations of the active site are seen in the presence of both AMP and ATP. Active conformation with ATP, dark blue; inactive conformation with ATP, light blue; active conformation with AMP, red; inactive conformation with AMP, pink; conformations of the two apo active sites; green and light green; and AMP-PNP as bound to DAPK1 in the active conformation, yellow. Note how the salt bridge between Lys42 and Glu64 breaks in the inactive conformation, coupled to changes in the water structure at this site. (b) Interactions of the basic loop from one DAPK2 monomer (blue) to the other (green). At the bottom right, a bound ATP is shown, under the P-loop. The basic loop is inserted into a groove between helices αG and αR1. Hydrogen bonds between Arg47, Arg50, and Arg53 and the opposing monomer are shown by orange broken lines.

family, the peptide-recognition region located around Phe178, is located in the center of the dimer interface of the crystal structure. Thus, both segments in the kinase domain sequence that are characteristic of the DAPK family are intimately involved in the dimerization of DAPK2.

The observation of the dimers both during purification and under the supersaturating conditions used in crystallization indicates that DAPK2 is able to dimerize; this was further proven by additional experiments (see below). On the other hand, if the dimers seen in the crystal structures are physiologically relevant, the binding of CaM prior to full activation must be coupled to the breaking of the dimerization of the catalytic domains as seen in the structure

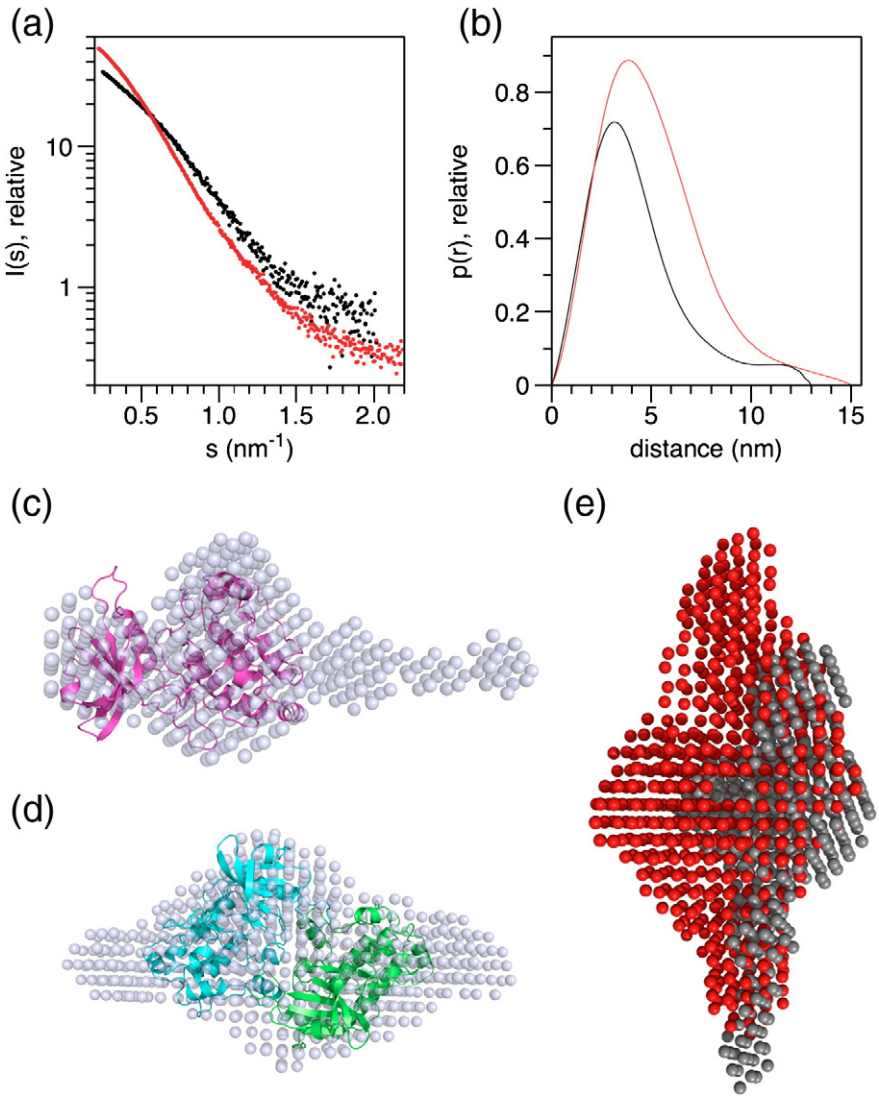

Fig. 5. Determination of the solution structure of DAPK2 by SAXS. (a) Scattering curves for the monomeric (black) and dimeric (red) forms. (b) Distance distribution functions. (c) Averaged *ab initio* model for the monomeric form of DAPK2; the crystal structure of a monomer (red) has been fitted into the envelope. (d) Averaged *ab initio* model for a DAPK2 dimer. The dimer, as seen in the crystal structure, has been fitted into the central part. (e) Comparison of the monomeric and dimeric SAXS models indicating how the monomeric form (black) takes up half of the volume and shape of the dimer (red). The superposition is based on first superimposing the dimeric crystal structure onto the dimer SAXS envelope and then superimposing the monomeric SAXS envelope onto one chain of the crystal structure; that is, the SAXS models *per se* have not directly been superimposed.

because the substrate peptide-binding surface is buried in the dimer interface and cannot be reached by a protein or peptide substrate destined for trans-phosphorylation. It is also possible that CaM binding requires the breaking of DAPK2 dimers by some other mechanism.

Solution structures of the different forms of DAPK2

The solution structures of monomeric and dimeric full-length DAPK2 were determined by synchrotron SAXS (Fig. 5 and Table 2), and the calculated

Table 2. SAXS results from the two peaks resolved by size-exclusion chromatography

Sample	$I(0)$	Molecular mass (kDa)[a]	R_g (nm)	D_{max} (nm)	Excluded volume (nm^3)	Molecular mass (kDa)[b]	χ[c]	Spatial discrepancy[d]
Monomer	43.0	58	3.45	13	61.2	48	0.9–1.0	1.8
Dimer	65.0	88 (1.5)[e]	3.98	15	122.4	95 (2.0)[e]	0.9–1.0	1.4

The expected molecular mass for a monomer is 42 kDa; the excluded volume is that for the averaged *ab initio* model.
[a] Calculated based on the $I(0)$ of a BSA standard.
[b] Calculated based on the excluded volume of a model correspondingly built for BSA.
[c] The χ values describe the fit of individual *ab initio* models, built using GASBOR, to the scattering data.
[d] The spatial discrepancy between superimposed SAXS and crystal structures, as reported by SUPCOMB after automatic superposition. It should be mentioned that the absence of the C-terminal tail in the crystal structure affects these values.
[e] Apparent molecular mass ratio between the dimeric and the monomeric fractions.

molecular weights confirmed the presence of monomeric and dimeric DAPK2 species. *Ab initio* models built for the monomeric form show the kinase catalytic domain and an extended tail (Fig. 5c). The monomeric crystal structure of the catalytic and autoinhibitory domains can be well fitted into the SAXS density. The presence of a long and at least partially disordered tail also explains the fact that the only crystals obtained, at least so far, represent a degradation product comprising the well-folded domain. The tail that is seen most likely corresponds to the C-terminal regulatory domain of DAPK2.

Model building for the DAPK2 dimer suggests a 2-fold symmetrical molecule, in which the catalytic domain dimer is in the middle, and the two C-terminal tails point out, away from each other (Fig. 5d and e). The dimeric crystal structure of DAPK2 fits well into the central part of the SAXS envelope. While it has been suggested that the C-terminal domain is required for dimerization,[3] it appears that the C-terminal tails are not directly mediating DAPK2 dimerization. It is possible that full-length DAPK2 has a higher affinity for dimerization than the catalytic domain alone.

Model for DAPK2 autophosphorylation and activation

Several levels of DAPK2 regulation are possible, ranging from gene regulation to cellular calcium levels and protein kinase signaling cascades. DAPK2 is known to be regulated by a double-locking mechanism, involving Ser308 autophosphorylation, CaM binding, and dimerization.[5] In the inactive state, Ser308 is phosphorylated, and the kinase is dimeric. For activation, Ser308 must be dephosphorylated; CaM needs to bind, displacing the autoinhibitory helix; and the kinase catalytic domain must become monomeric. The activated DAPK2 can then phosphorylate its physiological substrates, leading to cell death by apoptosis. To date, little data are available on the actual substrates of DAPK2, apart from its ability to phosphorylate myosin light chain and itself. In addition to its identified roles in erythropoiesis[8] and granulocyte maturation,[9] in recent studies, DAPK2 has been shown to be involved in the regulation of cell death in tumors induced by therapeutic agents. It is centrally involved in the epigallocatechin-3-gallate-induced cell death in acute myeloid leukemia,[38] and it is upregulated during the resveratrol-induced cell death of cancer stem-like cells isolated from breast cancer cell lines.[39] For a better understanding of these functions, a detailed structural analysis of the different states in the DAPK2 regulatory cascade must be carried out.

During the actual autophosphorylation event, Ser308 must act as a substrate in the active site. Indeed, through the use of the structures of DAPK2 and the PhK peptide complex as guides, a model can be built of the complex at the time of autophosphorylation (Fig. 6a). Continuing the chain onwards from Thr301, adding the three missing Arg residues 302–304 as a linker, and using the PhK peptide substrate (RQMSFRL) as a model [corresponding to DAPK2 residues 305–311 (WKLSFSI)], Ser308 comes exactly to the P0 position, and the sequence around it fits well into the peptide-binding surface, forming a β-sheet with region 177–180 of the DAPK2 large lobe. Interestingly, the same region of the regulatory tail will be in an α-helical conformation when bound by CaM during kinase activation.[22,40] In the model, Phe309 is inserted into the P+1 pocket, and Lys306 forms a salt bridge to Glu182 in the P-2 pocket. The three linker Arg residues 302–304 are positioned to interact with surrounding acidic residues, including Glu182, Asp220, Glu100, and Asp103.

The model explains well the observed autophosphorylation of DAPK2, as well as the observation that the ATP-binding site is accessible in DAPK2. Thus, we have now provided a structure of a dimeric form of DAPK2, which we believe to represent the inactive state of the kinase. Combined with a wealth of earlier data, including the crystal structure of CaM complexed to the CaM-binding domain of DAPK2[40] and the structure of the DAPK1–CaM complex in the inhibited conformation,[22] a scenario for DAPK2 regulation can now be envisaged at the structural level. Activation requires the dephosphorylation of Ser308; the binding of CaM to the CaM-binding domain, which is surrounded in the dimeric arrangement by a large positively charged patch (Fig. 6b); and generation of a monomeric active form of DAPK2 bound to CaM. A schematic view of DAPK2 activation is shown in Fig. 6c. We believe the regulation of the closely related kinases DAPK1 and ZIPK, both of which are known to dimerize, to follow a similar mechanism; in the case of ZIPK, factors other than CaM will be involved.

Concluding remarks

We have presented the first report on the three-dimensional structure of the pro-apoptotic kinase DAPK2, indicating dimerization and structural flexibility of the peptide-binding and active sites caused by the autoinhibitory domain and small-molecule ligands. The DAPK family is highly homologous within the catalytic domain, but the members differ significantly in their respective regulatory domains. Dimerization of the kinase has been observed for DAPK1, DAPK2, and ZIPK, and evidence suggests that this dimerization can occur through the catalytic domain alone. Our

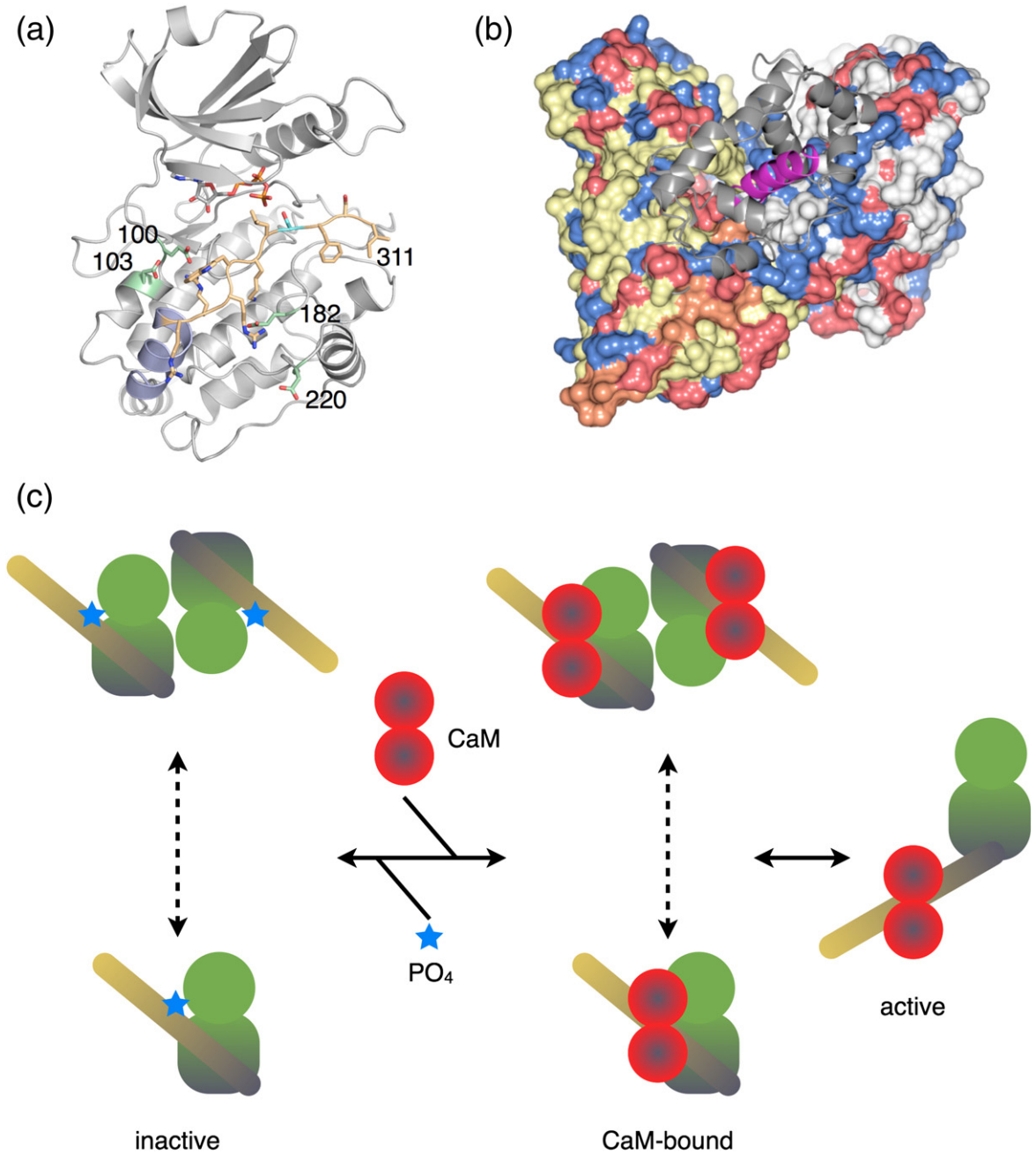

Fig. 6. Models for autophosphorylation and CaM regulation. (a) The model for autophosphorylation of Ser308. ATP is shown in the active site, and Ser308 is indicated in cyan; Phe309 is inserted into the P+1 pocket. The modeled part of the sequence, based on the PhK complex structure, is shown in light orange, and the autoinhibitory helix is in blue. Acidic residues involved in substrate recognition are indicated in green and numbered. (b) Surface representation of the DAPK2 dimer, with the two monomers colored yellow and white. The positions of basic (blue) and acidic (red) residues are indicated, and the autoinhibitory domain is otherwise colored orange, coming from the bottom left and ending in the middle. In the middle of the view, the CaM-binding segment (magenta) would emerge as an immediate continuation of the autoinhibitory helix; the surface of the dimer is highly positively charged around this site. The bound CaM, as seen in the corresponding peptide complex,[40] is modeled as a gray cartoon. (c) A schematic model for the different possible states in the regulation of DAPK2.

crystal and solution structures of DAPK2 provide a sensible model for homodimerization and heterodimerization in the DAPK family, centrally involving the fingerprint regions of this kinase subfamily. The structural data will provide a solid basis for further elucidation of DAPK2 function during

programmed cell death once its physiological substrates are identified.

Materials and Methods

Expression construct generation

The cDNA for mouse DAPK2 was purchased from RZPD (German Resource Center for Genome Research). The expression construct was made into the pTH27 vector[41] using the Gateway system (Invitrogen), as previously described for the human myelin P2 protein.[42] The primers used for DAPK2 insert amplification prior to Gateway cloning were 5′-AAAAAGCAGGCTCTGAGAATCTTTATTTTCAGGGCATGGAGACGTTCAAACAG-3′ and 5′-AGAAAGCTGGGTTCAGGAGGTACTGCTCCTC-3′. The resulting expression construct encoded for full-length mouse DAPK2 and an N-terminal His-tag, separated by a cleavage site for tobacco etch virus protease.

Protein expression and purification for crystallization

N-terminally His-tagged DAPK2 was expressed in *Escherichia coli* BL21 (DE3) pLysS Rare cells with the autoinduction method.[43] The cells were first cultured for 2 h at +37 °C, then cooled on ice, and further cultured at +20 °C for 36 h. The cells were harvested by centrifugation, and the pellet was resuspended in buffer A [50 mM Hepes (pH 7.5), 300 mM NaCl, and 10% glycerol] containing EDTA-free Complete protease inhibitors (Roche).

The cells were disrupted by sonication on ice, and the lysate was clarified by centrifugation at 18000*g* for 20 min. The clear lysate was applied onto a Ni-TED column pre-equilibrated with buffer A. The column was washed with 200 ml of buffer A, and DAPK2 was eluted with 250 mM imidazole in buffer A. The fractions were analyzed on SDS-PAGE for purity. Fractions containing DAPK2 were pooled and cleaved with recombinant tobacco etch virus protease[41] at +4 °C overnight.

The sample was concentrated, filtered, and injected into a pre-equilibrated size-exclusion column (Superdex S75). Size-exclusion chromatography was carried out in buffer A at a flow rate of 1 ml/min. The peak fractions were analyzed on SDS-PAGE, and the fractions of the apparent monomer peak were pooled and dialyzed against 20 mM Hepes, 100 mM NaCl, and 5 mM $CaCl_2$.

The sample was then applied onto a CaM agarose matrix (Sigma) pre-equilibrated with the same buffer. The column was washed extensively with the $CaCl_2$-containing buffer, and elution was carried out with the same buffer, with $CaCl_2$ replaced with 5 mM EDTA. The purified samples were analyzed by SDS-PAGE, and the buffer was exchanged by three rounds of concentration by centrifugal ultrafiltration and redilution to 20 mM Hepes (pH 7.5), 20 mM NaCl, and 10 mM DTT.

Protein expression and purification for X-ray and light scattering

The DAPK2 expression vector was transformed into *E. coli* Rosetta (DE3) pLacI cells. Overnight cultures were grown in 20 ml of LB with 100 μg/ml ampicillin and 34 μg/ml chloramphenicol at +37 °C. Two liters of ZYM-5052 autoinduction medium[43] were then inoculated. The cells were grown at +15 °C for 18 h; then, additional antibiotics (17 μg/ml chloramphenicol and 100 μg/ml ampicillin) and IPTG (2 mM) were added, and the culture was continued for another 34 h. The cells were then harvested by centrifugation.

The cells were resuspended in buffer B (50 mM Na phosphate, pH 8.0, and 300 mM NaCl) containing 20 mM imidazole and Complete protease inhibitors (Roche) and disrupted by sonication; cell debris were removed by centrifugation. The supernatant was applied onto a His-trap column (GE Healthcare). The matrix was washed with buffer B containing 40 mM imidazole, and elution of DAPK2 was performed using 250 mM imidazole in buffer B. The fractions were checked on SDS-PAGE and pooled. The samples were concentrated, and a final purification was performed by size-exclusion chromatography on a Superdex S200 16/60 column in 20 mM Hepes (pH 7.5), 50 mM NaCl, and 10% glycerol. Following chromatography, the fractions from the resolved peaks were separately pooled and concentrated.

Size-exclusion chromatography and static light scattering

Analytical size-exclusion chromatography was carried out using a Sephadex S200 10/30 column (GE Healthcare) coupled to an Äkta Purifier (GE Healthcare). The running buffer was 20 mM Hepes (pH 7.5), 50 mM NaCl, and 10% glycerol. The system was further attached to a mini-DAWN TREOS static light-scattering device (Wyatt) and an Optilab rEX differential refractometer (Wyatt) for absolute molecular weight determination. Molecular weights were determined based on the measured light scattering and refractive index using the ASTRA software (Wyatt).

Crystallization and data collection

For crystallization, the protein was in 20 mM Hepes (pH 7.5), 20 mM NaCl, and 10 mM DTT. DAPK2 was crystallized using the hanging-drop vapor diffusion method at +20 °C over a well solution of 0.1 M 2-[bis(2-hydroxyethyl)amino]-2-(hydroxymethyl)propane-1,3-diol (pH 6.0), 0.2 M Li_2SO_4, and 20% polyethylene glycol 3350. To obtain nucleotide complexes, we soaked the crystals for 20 min in drops containing 5 mM ATP or AMP, prepared in the well solution. Prior to data collection, the crystals were not treated with any additional cryoprotectants.

Data were collected at beamline ID14-2 of the European Synchrotron Radiation Facility (ESRF; Grenoble) and at beamline X12, European Molecular Biology Laboratory/Deutsches Elektronen Synchrotron (EMBL/DESY; Hamburg, Germany) in a cryostream of gaseous nitrogen at 100 K. All data were processed using XDS[44] and XDSi.[45]

Structure solution and refinement

The structure was solved by molecular replacement in Phaser[46] using the unpublished structure of human

DAPK2 kinase (Protein Data Bank entry 2A2A) as a model. Refinement was carried out in phenix.refine,[47] and manual model building was performed using Coot.[48] Non-crystallographic symmetry was not implemented during refinement between the two monomers of the asymmetric unit. The quality of the final structure was assessed using MolProbity.[34]

Small-angle X-ray scattering

The peaks resolved by size-exclusion chromatography, containing monomeric and dimeric full-length DAPK2, were further concentrated and subjected to synchrotron SAXS measurements for structural characterization. SAXS data from two separate batches of purified DAPK2 [in 20 mM Hepes (pH 7.5), 50 mM NaCl, and 10% glycerol] were collected on beamlines I711 at MAX-Lab, Lund, Sweden,[49] and X33 at EMBL/DESY. Primary data processing was carried out using the beamline software, and further processing and analysis were performed with the ATSAS package.[50] Specifically, distance distribution functions were calculated with GNOM,[51] and *ab initio* three-dimensional molecular models were built with DAMMIN,[52] DAMMIF,[53] and GASBOR.[54] Models were superimposed using SUPCOMB[55] and averaged using DAMAVER.[56] In averaging, the normalized spatial discrepancy of the individual *ab initio* models with respect to each other was between 1.2 and 1.7, indicating high level of similarity between the individual models. The molecular weight was estimated by means of comparing the forward scattering intensity $I(0)$ of the sample to that of a standard solution of bovine serum albumin (BSA). Another means to estimate the molecular weight consisted of the comparison of the volumes of the *ab initio* models of the samples and BSA.

Accession numbers

The refined coordinates and original diffraction data have been submitted into the Protein Data Bank under accession codes 2YA9 (apo), 2YAA (ATP complex), and 2YAB (AMP complex).

Supplementary materials related to this article can be found online at doi:10.1016/j.jmb.2011.03.065

Acknowledgements

We wish to thank the support staff at the used beamlines at ESRF, EMBL/DESY, and MAX-Lab and Prasad Kasaragod and Matti Myllykoski for participating in crystallographic data collection. This study was supported by grants from the Academy of Finland, Sigrid Jusélius Foundation (Finland), Boehringer Ingelheim Foundation (Germany), and German Academic Exchange Service (Germany). Data collection was supported by the European Community Seventh Framework Programme (FP7/2007-2013) under grant agreement 226716.

References

1. Shohat, G., Shani, G., Eisenstein, M. & Kimchi, A. (2002). The DAP-kinase family of proteins: study of a novel group of calcium-regulated death-promoting kinases. *Biochim. Biophys. Acta*, **1600**, 45–50.
2. Cohen, O., Feinstein, E. & Kimchi, A. (1997). DAP-kinase is a Ca^{2+}/calmodulin-dependent, cytoskeletal-associated protein kinase, with cell death-inducing functions that depend on its catalytic activity. *EMBO J.* **16**, 998–1008.
3. Inbal, B., Shani, G., Cohen, O., Kissil, J. L. & Kimchi, A. (2000). Death-associated protein kinase-related protein 1, a novel serine/threonine kinase involved in apoptosis. *Mol. Cell. Biol.* **20**, 1044–1054.
4. Kawai, T., Nomura, F., Hoshino, K., Copeland, N. G., Gilbert, D. J., Jenkins, N. A. & Akira, S. (1999). Death-associated protein kinase 2 is a new calcium/calmodulin-dependent protein kinase that signals apoptosis through its catalytic activity. *Oncogene*, **18**, 3471–3480.
5. Shani, G., Henis-Korenblit, S., Jona, G., Gileadi, O., Eisenstein, M., Ziv, T. *et al.* (2001). Autophosphorylation restrains the apoptotic activity of DRP-1 kinase by controlling dimerization and calmodulin binding. *EMBO J.* **20**, 1099–1113.
6. Shohat, G., Spivak-Kroizman, T., Cohen, O., Bialik, S., Shani, G., Berrisi, H. *et al.* (2001). The pro-apoptotic function of death-associated protein kinase is controlled by a unique inhibitory autophosphorylation-based mechanism. *J. Biol. Chem.* **276**, 47460–47467.
7. Inbal, B., Bialik, S., Sabanay, I., Shani, G. & Kimchi, A. (2002). DAP kinase and DRP-1 mediate membrane blebbing and the formation of autophagic vesicles during programmed cell death. *J. Cell Biol.* **157**, 455–468.
8. Fang, J., Menon, M., Zhang, D., Torbett, B., Oxburgh, L., Tschan, M. *et al.* (2008). Attenuation of EPO-dependent erythroblast formation by death-associated protein kinase-2. *Blood*, **112**, 886–890.
9. Rizzi, M., Tschan, M. P., Britschgi, C., Britschgi, A., Hugli, B., Grob, T. J. *et al.* (2007). The death-associated protein kinase 2 is up-regulated during normal myeloid differentiation and enhances neutrophil maturation in myeloid leukemic cells. *J. Leukoc. Biol.* **81**, 1599–1608.
10. Bandyopadhyay, S., Zhan, R., Wang, Y., Pai, S. K., Hirota, S., Hosobe, S. *et al.* (2006). Mechanism of apoptosis induced by the inhibition of fatty acid synthase in breast cancer cells. *Cancer Res.* **66**, 5934–5940.
11. Tur, M. K., Neef, I., Jager, G., Teubner, A., Stocker, M., Melmer, G. & Barth, S. (2009). Immunokinases, a novel class of immunotherapeutics for targeted cancer therapy. *Curr. Pharm. Des.* **15**, 2693–2699.
12. Tur, M. K., Neef, I., Jost, E., Galm, O., Jager, G., Stocker, M. *et al.* (2009). Targeted restoration of down-regulated DAPK2 tumor suppressor activity induces apoptosis in Hodgkin lymphoma cells. *J. Immunother.* **32**, 431–441.
13. Bialik, S. & Kimchi, A. (2004). DAP-kinase as a target for drug design in cancer and diseases associated with accelerated cell death. *Semin. Cancer Biol.* **14**, 283–294.

14. Yamakawa, A., Ogata, H., Morita, K., Shibata, N., Andou, N., Sanuki, H. *et al.* (2004). Crystallization and preliminary X-ray analysis of two inhibitor complexes of the catalytic domain of death-associated protein kinase. *Acta Crystallogr., Sect. D: Biol. Crystallogr.* **60**, 764–766.
15. Velentza, A. V., Wainwright, M. S., Zasadzki, M., Mirzoeva, S., Schumacher, A. M., Haiech, J. *et al.* (2003). An aminopyridazine-based inhibitor of a pro-apoptotic protein kinase attenuates hypoxia-ischemia induced acute brain injury. *Bioorg. Med. Chem. Lett.* **13**, 3465–3470.
16. Velentza, A. V., Schumacher, A. M. & Watterson, D. M. (2002). Structure, activity, regulation, and inhibitor discovery for a protein kinase associated with apoptosis and neuronal death. *Pharmacol. Ther.* **93**, 217–224.
17. Velentza, A. V., Schumacher, A. M., Weiss, C., Egli, M. & Watterson, D. M. (2001). A protein kinase associated with apoptosis and tumor suppression: structure, activity, and discovery of peptide substrates. *J. Biol. Chem.* **276**, 38956–38965.
18. Okamoto, M., Takayama, K., Shimizu, T., Muroya, A. & Furuya, T. (2010). Structure–activity relationship of novel DAPK inhibitors identified by structure-based virtual screening. *Bioorg. Med. Chem.* **18**, 2728–2734.
19. Okamoto, M., Takayama, K., Shimizu, T., Ishida, K., Takahashi, O. & Furuya, T. (2009). Identification of death-associated protein kinases inhibitors using structure-based virtual screening. *J. Med. Chem.* **52**, 7323–7327.
20. McNamara, L. K., Watterson, D. M. & Brunzelle, J. S. (2009). Structural insight into nucleotide recognition by human death-associated protein kinase. *Acta Crystallogr., Sect. D: Biol. Crystallogr.* **65**, 241–248.
21. Tereshko, V., Teplova, M., Brunzelle, J., Watterson, D. M. & Egli, M. (2001). Crystal structures of the catalytic domain of human protein kinase associated with apoptosis and tumor suppression. *Nat. Struct. Biol.* **8**, 899–907.
22. de Diego, I., Kuper, J., Bakalova, N., Kursula, P. & Wilmanns, M. (2010). Molecular basis of the death-associated protein kinase-calcium/calmodulin regulator complex. *Sci. Signal.* **3**, ra6.
23. Goldberg, J., Nairn, A. C. & Kuriyan, J. (1996). Structural basis for the autoinhibition of calcium/calmodulin-dependent protein kinase I. *Cell*, **84**, 875–887.
24. Rosenberg, O. S., Deindl, S., Sung, R. J., Nairn, A. C. & Kuriyan, J. (2005). Structure of the autoinhibited kinase domain of CaMKII and SAXS analysis of the holoenzyme. *Cell*, **123**, 849–860.
25. Mukherjee, K., Sharma, M., Jahn, R., Wahl, M. C. & Sudhof, T. C. (2010). Evolution of CASK into a Mg^{2+}-sensitive kinase. *Sci. Signal.* **3**, ra33.
26. Wernimont, A. K., Artz, J. D., Finerty, P. J., Lin, Y. H., Amani, M., Allali-Hassani, A. *et al.* (2010). Structures of apicomplexan calcium-dependent protein kinases reveal mechanism of activation by calcium. *Nat. Struct. Mol. Biol.* **17**, 596–601.
27. Mayans, O., van der Ven, P. F., Wilm, M., Mues, A., Young, P., Furst, D. O. *et al.* (1998). Structural basis for activation of the titin kinase domain during myofibrillogenesis. *Nature*, **395**, 863–869.
28. Hu, S. H., Parker, M. W., Lei, J. Y., Wilce, M. C., Benian, G. M. & Kemp, B. E. (1994). Insights into autoregulation from the crystal structure of twitchin kinase. *Nature*, **369**, 581–584.
29. Padre, R. C. & Stull, J. T. (2000). Conformational requirements for Ca^{2+}/calmodulin binding and activation of myosin light chain kinase. *FEBS Lett.* **472**, 148–152.
30. Mukherji, S., Brickey, D. A. & Soderling, T. R. (1994). Mutational analysis of secondary structure in the autoinhibitory and autophosphorylation domains of calmodulin kinase II. *J. Biol. Chem.* **269**, 20733–20738.
31. Tanaka, M., Ikebe, R., Matsuura, M. & Ikebe, M. (1995). Pseudosubstrate sequence may not be critical for autoinhibition of smooth muscle myosin light chain kinase. *EMBO J.* **14**, 2839–2846.
32. Fitzsimons, D. P., Herring, B. P., Stull, J. T. & Gallagher, P. J. (1992). Identification of basic residues involved in activation and calmodulin binding of rabbit smooth muscle myosin light chain kinase. *J. Biol. Chem.* **267**, 23903–23909.
33. Lowe, E. D., Noble, M. E., Skamnaki, V. T., Oikonomakos, N. G., Owen, D. J. & Johnson, L. N. (1997). The crystal structure of a phosphorylase kinase peptide substrate complex: kinase substrate recognition. *EMBO J.* **16**, 6646–6658.
34. Chen, V. B., Arendall, W. B. r., Headd, J. J., Keedy, D. A., Immormino, R. M., Kapral, G. J. *et al.* (2010). MolProbity: all-atom structure validation for macromolecular crystallography. *Acta Crystallogr., Sect. D: Biol. Crystallogr.* **66**, 12–21.
35. Shani, G., Marash, L., Gozuacik, D., Bialik, S., Teitelbaum, L., Shohat, G. & Kimchi, A. (2004). Death-associated protein kinase phosphorylates ZIP kinase, forming a unique kinase hierarchy to activate its cell death functions. *Mol. Cell. Biol.* **24**, 8611–8626.
36. Zimmermann, M., Atmanene, C., Xu, Q., Fouillen, L., Van Dorsselaer, A., Bonnet, D. *et al.* (2010). Homodimerization of the death-associated protein kinase catalytic domain: development of a new small molecule fluorescent reporter. *PLoS One*, **5**, e14120.
37. Bahadur, R. P., Chakrabarti, P., Rodier, F. & Janin, J. (2004). A dissection of specific and non-specific protein–protein interfaces. *J. Mol. Biol.* **336**, 943–955.
38. Britschgi, A., Simon, H. U., Tobler, A., Fey, M. F. & Tschan, M. P. (2010). Epigallocatechin-3-gallate induces cell death in acute myeloid leukaemia cells and supports all-trans retinoic acid-induced neutrophil differentiation via death-associated protein kinase 2. *Br. J. Haematol.* **149**, 55–64.
39. Pandey, P. R., Okuda, H., Watabe, M., Pai, S. K., Liu, W., Kobayashi, A. *et al.* (2010). Resveratrol suppresses growth of cancer stem-like cells by inhibiting fatty acid synthase. *Breast Cancer Res. Treat.*; [Epub ahead of print].
40. Bertini, I., Kursula, P., Luchinat, C., Parigi, G., Vahokoski, J., Wilmanns, M. & Yuan, J. (2009). Accurate solution structures of proteins from X-ray data and a minimal set of NMR data: calmodulin–peptide complexes as examples. *J. Am. Chem. Soc.* **131**, 5134–5144.

41. Hammarstrom, M., Woestenenk, E. A., Hellgren, N., Hard, T. & Berglund, H. (2006). Effect of N-terminal solubility enhancing fusion proteins on yield of purified target protein. *J. Struct. Funct. Genomics*, **7**, 1–14.
42. Majava, V., Polverini, E., Mazzini, A., Nanekar, R., Knoll, W., Peters, J. *et al.* (2010). Structural and functional characterization of human peripheral nervous system myelin protein P2. *PLoS One*, **5**, e10300.
43. Studier, F. W. (2005). Protein production by auto-induction in high density shaking cultures. *Protein Expression Purif.* **41**, 207–234.
44. Kabsch, W. (1993). Automatic processing of rotation diffraction data from crystals of initially unknown symmetry and cell constants. *J. Appl. Crystallogr.* **26**, 795–800.
45. Kursula, P. (2004). XDSi: a graphical interface for the data processing program XDS. *J. Appl. Crystallogr.* **37**, 347–348.
46. McCoy, A. J., Grosse-Kunstleve, R. W., Adams, P. D., Winn, M. D., Storoni, L. C. & Read, R. J. (2007). Phaser crystallographic software. *J. Appl. Crystallogr.* **40**, 658–674.
47. Adams, P. D., Afonine, P. V., Bunkoczi, G., Chen, V. B., Davis, I. W., Echols, N. *et al.* (2010). PHENIX: a comprehensive Python-based system for macromolecular structure solution. *Acta Crystallogr., Sect. D: Biol. Crystallogr.* **66**, 213–221.
48. Emsley, P. & Cowtan, K. (2004). Coot: model-building tools for molecular graphics. *Acta Crystallogr., Sect. D: Biol. Crystallogr.* **60**, 2126–2132.
49. Cerenius, Y., Stahl, K., Svensson, L. A., Ursby, T., Oskarsson, A., Albertsson, J. & Liljas, A. (2000). The crystallography beamline I711 at MAX II. *J. Synchrotron Radiat.* **7**, 203–208.
50. Konarev, P. V., Petoukhov, M. V., Volkov, V. V. & Svergun, D. I. (2006). ATSAS 2.1, a program package for small-angle scattering data analysis. *J. Appl. Crystallogr.* **39**, 277–286.
51. Svergun, D. I. (1992). Determination of the regularization parameter in indirect-transform methods using perceptual criteria. *J. Appl. Crystallogr.* **25**, 495–503.
52. Svergun, D. I. (1999). Restoring low resolution structure of biological macromolecules from solution scattering using simulated annealing. *Biophys. J.* **76**, 2879–2886.
53. Franke, D. & Svergun, D. I. (2009). DAMMIF, a program for rapid *ab-initio* shape determination in small-angle scattering. *J. Appl. Crystallogr.* **42**, 342–346.
54. Svergun, D. I., Petoukhov, M. V. & Koch, M. H. (2001). Determination of domain structure of proteins from X-ray solution scattering. *Biophys. J.* **80**, 2946–2953.
55. Kozin, M. & Svergun, D. I. (2000). Automated matching of high- and low-resolution structural models. *J. Appl. Crystallogr.* **34**, 33–41.
56. Volkov, V. V. & Svergun, D. I. (2003). Uniqueness of *ab initio* shape determination in small angle scattering. *J. Appl. Crystallogr.* **36**, 860–864.